Analyst

PAPER

View Article Online
View Journal | View Issue

Cite this: *Analyst*, 2019, **144**, 6953

A miniaturized electrochemical platform with an integrated PDMS reservoir for label-free DNA hybridization detection using nanostructured Au electrodes†

Suryasnata Tripathy,‡[a] Jose Joseph,‡[a] Saketh Pothuneedi,[a] Dhruv Das,[b] Siva Rama Krishna Vanjari,[a] A. V. S. S. Narayana Rao[b] and Shiv Govind Singh *[a]

We report the fabrication and characterization of a miniaturized electrochemical platform for the label-free detection of DNA hybridization. The proposed platform is fabricated using microfabrication and electrodeposition techniques. Comprising a Ti working electrode with electrodeposited Au nanostructures, and Pt/Au pseudo-reference and counter electrodes, the device accounts for a limit of detection of 0.97 fM and a sensitivity of 20.78 (μA μM^{-1}) cm^{-2} with respect to Dengue virus specific consensus primer detection in the range of 10 fM–1 μM. Here, the incorporation of nanostructured Au in the active sensing area not only enhances the current response by increasing the overall surface area, but it also facilitates facile probe DNA immobilization by gold–thiol self-assembly. We have used differential pulse voltammetry analysis in this study to monitor the changes in reaction kinetics with respect to target hybridization. Furthermore, the evaluation of reproducibility of the biosensor and its selectivity against interference has yielded acceptable outcomes. Additionally, in order to evaluate the system's selectivity, we have successfully distinguished PCR amplified wild type and mutant target DNAs corresponding to the BRCA1 specific gene. Here, the mutant and the wild type target DNAs differ by a two base deletion, and the fact that the system is able to differentiate even such minute dissimilarities under hybridization conditions is indicative of its superior performance.

Received 12th June 2019,
Accepted 21st September 2019

DOI: 10.1039/c9an01076a

rsc.li/analyst

Introduction

Point-of-care disease diagnosis often requires the development of miniaturized platforms that can provide high accuracy and selectivity. In this context, the precise and quantitative detection of DNA hybridization for the diagnosis of infections and genetic disorders is an important field of study. For example, the detection of Dengue virus (DENV) specific DNAs is of tremendous clinical significance given the severity of the disease across the globe.[1] Ensuring the detection of DENV in low concentrations can ensure early diagnosis of the viral infection, and allow patients to get timely medical attention. Also, the development of a simple and economic alternative to the commercially available rapid detection test kits may be vital for the diagnosis of DENV infection, particularly in developing countries. Likewise, the detection of genetic disease specific mutations is of importance. Keeping this in mind, the current work is directed towards developing a miniaturized biosensing platform, for DNA hybridization detection.

In general, in most DNA sensors, a single stranded target DNA is detected using its complementary single stranded probe nucleotide as the capturing agent. The probe, in essence, forms a hybridization complex with the target nucleotide. Towards the quantitative detection of a hybridization event, the same is recorded using suitable transduction principles.[2–5] A correlation is then established between the transduced signal (be it optical, mechanical or electrical) and the hybridization conditions, and an empirical relation is derived. In essence, the quality of the transduction principle, among other factors, is largely determined by its resolution, which is its ability to distinguish closely related biological events. Furthermore, the scalability of any sensing platform is of great importance, as this holds the key to developing economic and portable diagnostic tools. In the past, label-free electrochemical biosensors have been extensively used in such applications on account of their sensitivity and amenability to miniaturization.[6–13] Previously, we have also reported several such biosensing platforms that have targeted single stranded

[a]*Indian institute of technology, Hyderabad, India-502285. E-mail: sgingh@iith.ac.in*
[b]*Bhabha atomic research centre, Mumbai, India-400 085*

†Electronic supplementary information (ESI) available. See DOI: 10.1039/c9an01076a

‡These authors have contributed equally.

target DNA detection for disease diagnosis and genetic studies.[14–16] However, those sensors were realized as macro systems, and their miniaturization for point-of-care diagnosis was left to be addressed. In lieu of this, in the present work, we have developed a miniaturized electrochemical biosensor, wherein the working electrode comprises electrodeposited gold nanostructures.

Historically, gold working electrodes have been used in DNA biosensing as they provide an efficient, yet simple, means of surface functionalization *via* thiol self-assembly.[17–19] In addition to this, the usage of Au nanostructures provides one with the added advantage of increased surface area, which in turn enhances the overall system response. We have also exploited such benefits in the proposed platform. Additionally, we have provided an efficient fabrication process flow for scaling down the same. In the literature, this has not been widely explored for point of care DNA sensing. Here, we have developed the desired Au nanostructures using the technique of electrodeposition, as described previously.[16,20] Of note, we have experimentally optimized the said protocol to attain the most favourable performance. A more detailed analysis relating to Au electrodeposition on Ti can be found in the literature.[21] In this work, using the standard CMOS fabrication system, we have confined the entire sensor platform on a rectangular Si piece (3 cm × 1.5 cm), to conceive the miniaturized on-chip system. Towards connecting the sensor with the electrochemical workstation, we have used a micro-USB based interfacing assembly. Furthermore, for creating a reaction chamber, we have used a PDMS reservoir, which has been attached to the miniaturized biochip using organic adhesives. This idea has been inspired by the work carried out previously by Ian Papautsky and group.[22] In subsequent sections, the overall fabrication process flow has been described in detail. Of note, attempts at developing lab on chip systems for DNA biosensing are not new, and the related research is blossoming day by day.[23–26] A large fraction of the same is based on labelled transduction schemes. In this study, we present our take on developing a miniaturized lab on chip platform involving label free electrochemical transduction, a novel microfabrication protocol and a simple electrodeposition step. In order to demonstrate the proposed system's efficiency in DNA hybridization detection in general, and disease diagnosis in particular, thiolated DNA probes specific to the DENV consensus primer (DENVCP) have been used in this study. Of note, the consensus primer has been selected for the analysis, as it is a representative nucleotide sequence of all four dengue virus serotypes. Here, the thiolated probes are immobilized on the working electrode to serve as the capturing agent for the complementary target DNA. The concentration dependent probe–target hybridization event was recorded and interpreted using differential pulse voltammetry (DPV). A schematic representation of the proposed sensing protocol is presented in Fig. 1. In addition to this, we have evaluated the system's efficiency in differentiating wild type and mutant DNAs with two base deletion. This is essential in order to define the system's selectivity, which is a critical parameter in establishing its performance. For this, we have designed experiments involving the BRCA1 gene specific delAG mutation. The BRCA1 gene (OMIM: 113705) is located on chromosome 17q21.31 and is shown to predispose to familial breast cancer.[27] 185delAG (NC_000017.11: g.43124030_43124031delCT) is one of the founder mutations present in exon 2 of BRCA1.[28] This deletion leads to a change in the amino acid sequence of BRCA1 from glutamate (Glu) at position 23 to valine (Val), followed by a stop codon. This is represented as Glu23Valfs (BRCA1 NP_009225.1:p.E23Vfs). In light of the severe effects of this deletion, we have previously attempted detecting the same using metal oxide nanofiber based electrochemical transduction.[15] In this work, we intend to demonstrate the same using PCR amplified 185delAG positive and wild type DNA samples. This is one step closer to the real time scenario, which involves PCR products.

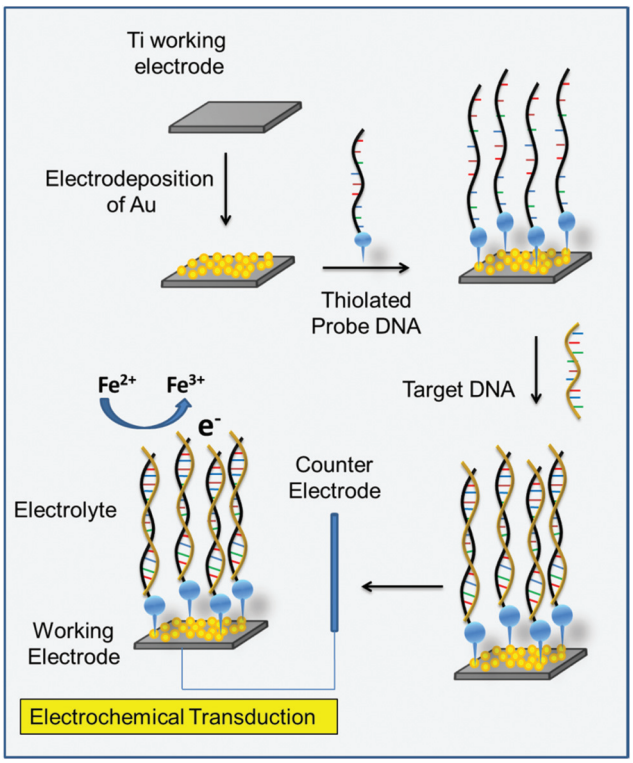

Fig. 1 Schematic representation of the Au nanostructure based working electrode fabrication and the subsequent DNA immobilization protocol. A conceptual representation of the electrochemical transduction process has also been provided.

Experimental

Materials and apparatus

For this work, the required chemicals such as chloroauric acid ($HAuCl_4$), sodium sulphate (Na_2SO_4), bovine serum albumin (BSA), human serum albumin (HSA) and phosphate buffered saline (PBS tablets) were purchased from Sigma Aldrich, USA. Towards fabricating the miniaturized sensor units, micro USB

connectors were purchased from Avishkar Innovative Pvt. Ltd, Bengaluru, India. In order to facilitate the morphological studies of the electrodeposited gold film, a scanning electron microscope (Carl Zeiss) was used in this study. Towards the electrochemical analysis carried out in this paper, we have used a CH660E workstation (CH Instruments). The target DNA locus amplification was done using the Mastercycler® epgradient S system from Eppendorf.

Probe and target DNAs

For the BRCA1 gene related experiments involving PCR products, we designed a primer pair such that the product amplified spans the 185delAG mutation. The size of the PCR product is 346 bp. The probe designed for conducting electrochemical assays is complementary to the mutant 185delAG BRCA1 sequence. The nucleotide sequence along with the chromosomal coordinates of the PCR product in the BRCA1 gene and the probe complementary sequence (for probe and primer sequence details, see Table 1) are given below:

(43123785)TTATCTGCTCTTCGCGTTGAAGAAGTACAAAATG-*TCATTAATGCTATGCAGAAAATCTT***AG***AGTGTCCCATCTGGTAAG-TCAGCAC*AAGAGTGTATTAATTTGGGATTCCTATGATTATCTCC-TATGCAAATGAACAGAATTGACCTTACATACTAGGGAAGAAAAG-ACATGTCTAGTAAGATTAGGCTATTGTAATTGCTGATTTTCTTAA-CTGAAGAACTTTAAAAATATAGAAAATGATTCCTTGTTCTCCATC-CACTCTGCCTCTCCCACTCCTCTCCTTTTCAACACAAATCCTG-TGGTCC(43124090)

Underlined: forward and reverse primer binding sites;

Underlined italics: probe complementary sequence;

Bold Red: 185delAG mutation location

For this study, two PCR fragments containing 185delAG mutation were obtained from Dr Rajiv Sarin of the Advanced Centre for Treatment, Research and Education in Cancer (ACTREC), Navi Mumbai. Furthermore, two BRCA1 wild type DNA samples were extracted from two BRCA1 wild type cell lines, namely H1975 and A549 (both are lung cancer cell lines, also obtained from ACTREC). For the del185AG locus amplification, in each PCR reaction, 50 ng of the template DNA was added to 20 μL of the reaction mixture consisting of 1× Universal PCR Premix (Genome Diagnostics Pt. Ltd.). Both forward and reverse primers (sequences of the primers are given in the Table 1) were added at 5.0 μmol L^{-1}. The PCR reaction consisted of an initial denaturation of 3 min at 95 °C, followed by 35 cycles of 20 s of denaturation at 94 °C, 20 s of annealing at 50 °C, and 30 s of extension at 72 °C, and a final extension step of 5 min at 72 °C. After the reaction, the PCR product was mixed with 1 μL of 6× loading dye and then separated on 2% agarose gel (3 μL of 0.5 mg L^{-1} ethidium bromide added in 70 mL of Tris-acetate-EDTA buffer) by routine submerged electrophoresis (70 V, 60 min) and viewed under ultraviolet illumination. As shown in Fig. 2, both the del185AG mutant and wild type PCR products (346 bp) were successfully amplified using the designed primer pair.

Fabrication of the miniaturized electrochemical platform

The on-chip sensing platform evolved as a result of several design optimizations and fabrication iterations. Keeping the flexibility aspect in mind, the proof of concept of DNA hybridization detection using gold nanostructures on a ITO coated PET substrate was initially demonstrated.[16] Following this, an on-chip electrochemical platform was developed using microfabrication techniques. As a step closer to lab-on-chip demonstrations, we incorporated a PDMS reservoir on the sensing platform. This will eventually bring down the quantity of analyte required for the DNA hybridization detection experiments (here, we have used an electrolyte volume of 100 μL),

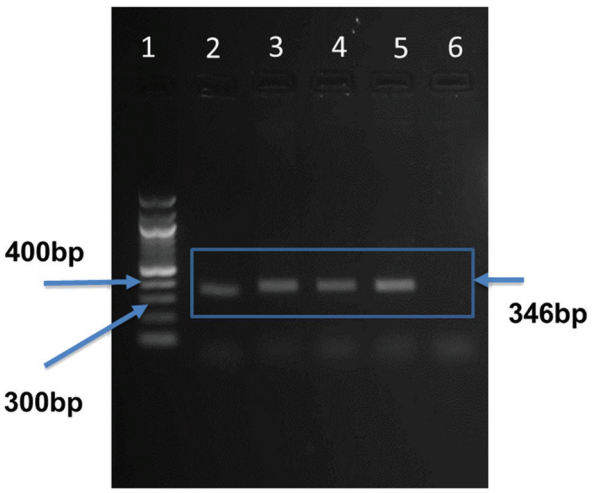

Fig. 2 Four PCR products (two positive for del185AG mutation and two negative for del185AG mutation) of 346 bp size were amplified. Samples were analysed on a 2% TAE agarose gel and visualized by staining with ethidium bromide. From left to right the sequence of loading is as follows: Lane 1: DNA ladder, Lane 2: del185AG positive sample, Lane 3: del185AG positive sample, Lane 4: A549 (del185AG negative), Lane 5 H1975 (del185AG negative), Lane 6: negative template control (NTC).

Table 1 Probe and primer details for the PCR experiment

Oligonucleotide	Sequence	Length
Forward primer[a]	cactggccgtcgttttacaTTATCTGCTCTTCGCGTTG	38
Reverse primer[b]	caggaaacagctatgaccatg GGACCACAGGATTTGTGTTGA	42
Probe	GTGCTGACTTACCAGATGGGACACTAAGATTTTCTGCATAGCATTAATGA	50

[a] Forward primer comprises a 19 bp extra sequence (adapter sequence) at the 5′-end not complimentary to any sequence in the human genome. [b] Reverse primer comprises a 21 bp extra sequence (adapter sequence) at the 5′-end not complimentary to any sequence in the human genome.

and also ensure uniformity in sample delivery. Briefly, silicon wafer pieces of dimension 3 cm × 1.5 cm were cleaved out of a 4-inch oxidized wafer to fabricate the biochip. After performing standard wafer cleaning processes, 50 nm titanium was deposited on the wafer pieces using an E-beam evaporation system (VST, Israel). This was then patterned in the shape of the working, counter and reference electrodes as shown in Fig. 3. Here, we have used a 2 mm diameter working electrode, a 1.5 mm wide reference and 0.7 mm wide counter electrode, where the inter-electrode distance (working-counter and working-reference) was kept as 500 μm. Towards creating the counter and pseudo-reference electrodes, 50 nm platinum was selectively deposited at desired places using a positive photoresist assisted lift-off. The sensing part of the working electrode was protected in this step with the photoresist to avoid any platinum deposition. In the third lithographic step, all the metal regions except the active regions and bond pads of the electrodes were protected by SU-8. This is performed to ensure desired isolation. Subsequently, for the electrodeposition of Au nanostructures, an electrochemical cell comprising the fabricated Ti working electrode, a Pt wire counter electrode and an Ag/AgCl reference electrode was used. 5 mM $HAuCl_4$ in 0.1 M Na_2SO_4 was used as the electrolyte for the desired electrochemical deposition. For the sensing work, the deposition of Au nanostructures on to the Ti surface was performed at a constant potential of −1 V for a period of 60 seconds. Since the electro-deposition process on the working electrode is a highly selective process, it did not affect the active regions of the other electrodes. Post electro-deposition, the micropatterned electrode was thoroughly washed, followed by IPA treatment and N_2 drying. Of note, the proposed process flow is a novel technique to fabricate a miniaturized electrochemical biosensor with nanostructured Au working electrodes.

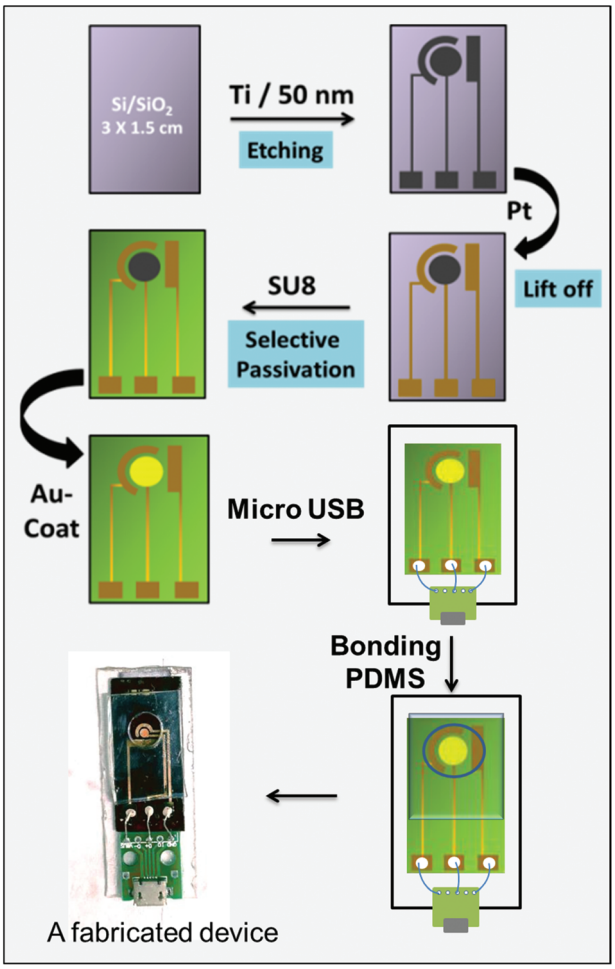

Fig. 3 Schematic representation of the process flow for the miniaturized electrochemical biosensor platform fabrication. A miniaturized and micro USB connected device, after the PDMS reservoir integration, has also been shown.

Towards realizing the end-goal of this research, which is to develop a portable electrochemical lab-on-chip platform for DNA hybridization detection, interfacing the sensor with necessary electronics is essential. To achieve this, electrical connections have to be taken out from the electrodes, such that the system can be paired with a read-out platform in future. Keeping this in mind, in this study we have used a micro-USB based interfacing, which can easily be connected to several computing platforms such as laptops, desktops and mobile phones, using their inbuilt USB ports. Furthermore, a standalone readout device can be designed in future which entertains USB based interfacing through a simple plug-in mechanism, such that the same device can be used for several sensing units. For this purpose, in this study, the fabricated chip was attached onto a transparent acrylic board of dimensions 5 cm × 2 cm. A standard micro-USB male port was then attached onto the acrylic board and necessary electric connections were established between the electrodes and the micro-USB *via* wire bonding. Towards this, we have used an in-house developed method, wherein one end of the conducting wires was attached on to the device's bond pads with the help of silver paste, while the other end was shouldered on to the PCB mount micro-USB. For the initial testing, the device was connected to a CHI 660E electrochemical workstation *via* the micro USB, using a USB–USB interface. The experimental setup is presented in Annexure 1 of the ESI.† Towards realizing the sensing chamber, a PDMS reservoir was created on the sensing platform by bonding a PDMS block with a cavity of 6 mm diameter, which aligned with the sensing area of the platform. For this, the PDMS film was created using a 10 : 1 ratio of the polymer and the curing agent. Post thermal treatment, the reservoirs were implanted on the cured film using a through-punch process. The same was attached to the sensor strip using organic adhesive assisted thermal bonding. A schematic representation of the process flow, along with a photograph of the miniaturized on-chip detection platform, is shown in Fig. 3.

Protocols for DNA sensing

As part of the first case study, thiolated probe DNA (thiol-CGG TTT CTC GCG CGT TTC AGC ATA TTG A, 5′-3′, Bioserve technologies, India), complementary to DENVCP target DNA (TCA ATA TGC TGA AAC GCG CGA GAA ACC G; 5′-3′), was immobi-

lized on the working electrode. To facilitate the biofunctionalization, the Ti/Au working electrode was incubated in a buffer solution containing 1 μM of the thiolated probe DNA for 24 h at 4 °C. During this period, the self-assembly of thiol groups on gold ensured the desired immobilization. Towards confirming the accuracy of the incubation time, we performed fluorescence microscopy (using the Carl Zeiss Z1 fluorescence microscope) on probe DNA immobilized gold substrates. For this, FITC labeled DNA probes were procured from Bioserve technologies, and Au substrates were incubated with the same for 24 h at 4 °C. The corresponding results, as presented in Fig. 4, indicate successful immobilization of the probe DNAs, substantiating the protocol. Subsequently, the electrodes (Ti/Au/probe) were thoroughly rinsed with PBS buffer and DI water, to remove the unbound nucleotides. Post probe-DNA hybridization, the bioelectrodes were treated with BSA for blocking the nonspecific adsorption sites. Subsequently, the electrodes were washed, dried with N_2 and stored under refrigeration until further use.

Towards the target DNA hybridization, the Ti/Au/probe electrodes were incubated in a buffer solution containing different concentrations of the target DNA at 37 °C for 1 h. In a previous study, we have reported about optimizing the incubation period for probe–target hybridization.[15] Post-incubation, the electrodes were rinsed with PBS buffer, so as to remove any unbound target nucleotides. For the interference study undertaken in this work, as part of the first case study involving DENVCP, the Ti/Au/probe electrode's response was recorded in the presence of two interfering agents: 10 nM of a noncomplementary DNA (NC) of similar length and 1 μg mL^{-1} human serum albumin (HSA). Furthermore, the electrode's response to 10 nM target DNA was recorded in the presence of both these molecules for a clearer understanding.

As part of the second case study, where BRCA1 gene specific hybridization detection was targeted, we used PCR modified target DNAs specific to a single stranded probe (see Table 1). This exercise was designed to evaluate the sensor's performance against patient-like samples, thereby bringing our efforts one step closer to the real-time application. Here, the probe DNA (1 μM) was attached on to the Au working electrodes using NHS/EDC chemistry, *via* a self-assembled monolayer of mercaptopropionic acid (MPA). MPA has previously been reported to form self-assembly on gold *via* its thiol groups, which leaves behind the carboxylic acid groups for subsequent functionalization steps.[29–31] The same can be then subjected to suitable chemistry for probe DNA hybridization. The protocol for such a surface modification protocol has been explained previously by our group.[14,15] The probe modified electrodes were later challenged with two distinct PCR products, where one was with the intended delAG mutation (complementary to the probe) and the other was a wild type sequence (2 base mismatch with the probe). Of note, the PCR products are double stranded in nature, whereas the probe DNA is a single stranded entity. To facilitate hybridization, prior to their incubation, the target DNAs were subjected to 2 min of heat treatment at 90 °C, followed by immediate chilling in ice. Furthermore, we have used a diluted (1 : 100) version of the PCR output, so as to minimize the effect of the PCR buffer (with high salt concentration) on the device's response.

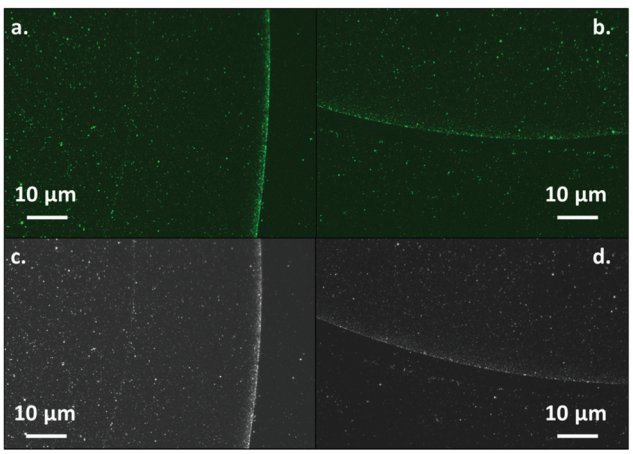

Fig. 4 Fluorescence microscopy images of the FITC tagged probe DNAs immobilized onto gold substrates *via* gold–thiol self-assembly, for probe DNA concentrations (a) 10 μM and (b) 1 μM. Figure (c) and (d) are the grey scale representations of figure (a) and (b), respectively.

Results and discussion

Characterization of the Au nanostructure based working electrode

Surface morphology. The structure of the miniaturized electrochemical platform was investigated using a scanning electron microscope (SEM, Carl Zeiss, Germany). The same can be seen in Fig. 5(a and b). Fig. 5(c) shows the micrograph of the silver paste assisted electrical inter-connection between

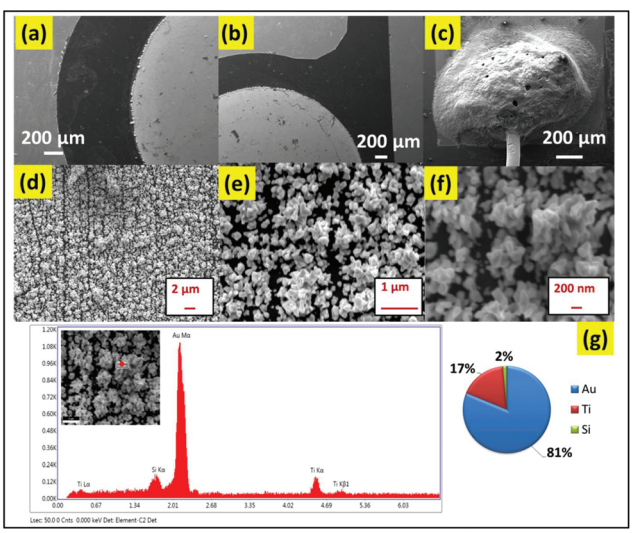

Fig. 5 SEM images of (a–b) the miniaturized electrochemical platform showing different electrodes, (c) the silver paste assisted electrical interconnection at a bond pad, (d–f) the electrodeposited gold nanostructures at different magnifications; (f) EDX results of a point analysis performed on the gold nanostructure.

the fabricated microelectrodes and a connecting wire. The surface morphology of the Ti/Au electrodes was also analyzed using SEM. As shown in Fig. 5(d–f), under the selected deposition conditions, a reasonably good surface coverage is achieved. Also, the electrodeposition resulted in the formation of nanoflower like Au structures which results in a large surface area. The effect of deposition time and deposition voltage on the electrodeposition of Au nanostructures on conducting surfaces has been discussed in our previous communication.[16] Therein, we had performed experimentation on ITO coated flexible substrates, and had optimized the deposition parameters for desired surface coverage and morphology. With reference to that, in the present study, we performed the electrodeposition at −1 V for a period of 60 seconds on to the Ti working electrodes. The energy-dispersive X-ray spectroscopy (EDX) results presented in Fig. 5(g) show distinct peaks corresponding to Au and Ti, along with a peak attributed to the Si substrate. This is a confirmation of successful Au deposition on the Ti working electrodes. We have also presented the Raman spectroscopy analysis (WItec, λ: 532 nm) results of the electrodeposited Au nanostructures in Annexure 2 of the ESI.†

In relation to the electrodeposition process, the cyclic voltammogram of the Ti deposited electrodes in 5 mM $HAuCl_4$ (in 0.1 M Na_2SO_4) and the current-time graphs are presented in Annexure 3 (Fig. 3) of the ESI.† Post Au deposition, the electrode response towards the redox activity of the Fe^{2+}/Fe^{3+} couple is significantly enhanced as opposed to the bare Ti electrode, and the same has been highlighted in Annexure 3 (Fig. 4) of the ESI.† We have also investigated the effect of different deposition conditions on the electrode's analytical performance, and the same has been presented in Annexure 3 (Fig. 5) of the ESI.†

Towards the electrochemical characterization of the bare electrodes, we performed cyclic voltammetry measurements in 0.1 M phosphate buffered saline, containing a 5 mM $[Fe(CN)_6]^{3-/4-}$ redox couple. As presented in Fig. 6(a), the corresponding cyclic voltammograms show a sigmoidal behaviour. Such behaviour is characteristic of micro-structured electrodes, where on account of significant radial diffusion, a steady state is realized between the diffusion and the electron transfer.[16,32] As can be seen, here, both the anodic and the cathodic peak currents increase with increasing scan rate. Also, with increasing scan rate, only the peak currents

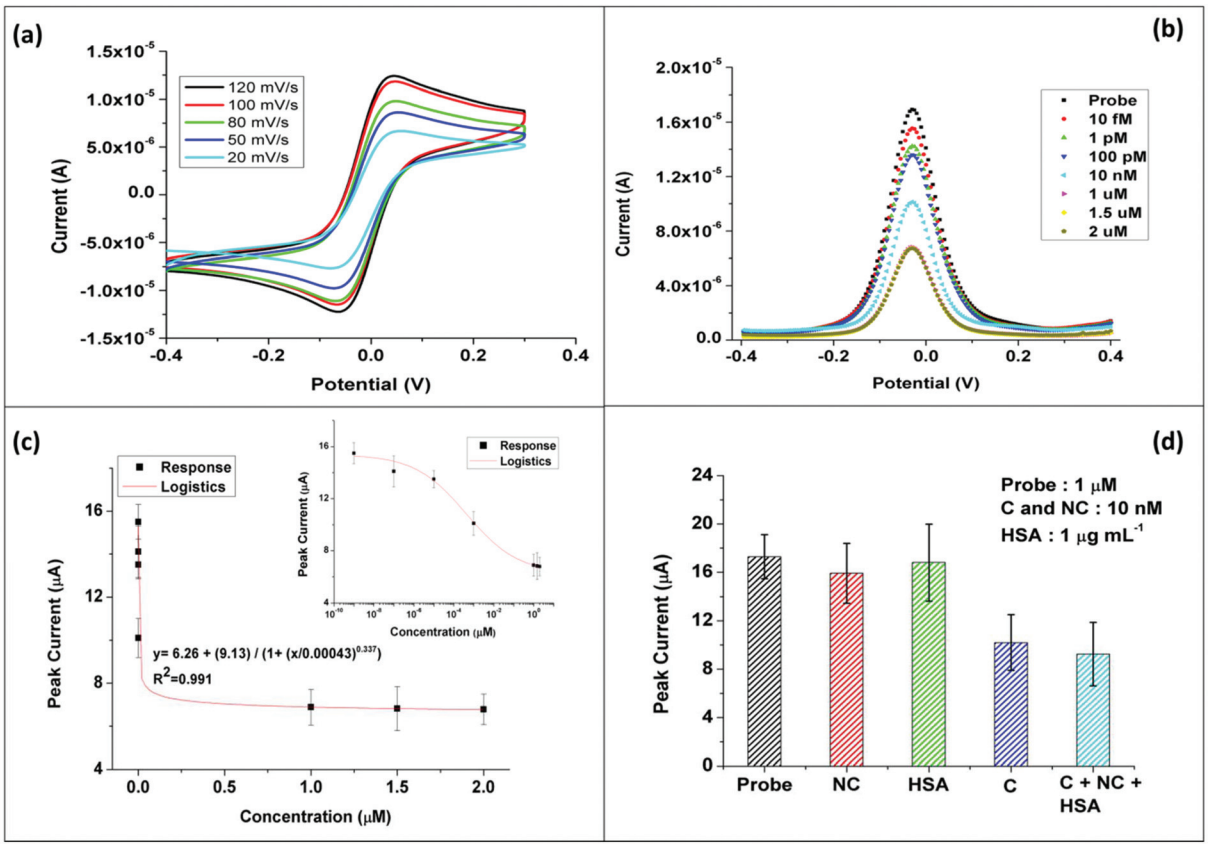

Fig. 6 (a) Cyclic voltammograms of the Ti/Au working electrode for different scan rates, (b) differential pulse voltammograms for the Ti/Au/probe electrode against different target concentrations, (c) calibration curve for the proposed DNA sensor showing the variation of peak currents with the target concentration, along with a four parameter logistics fit. Inset is the calibration curve with a logarithmic *x*-axis. (d) Interference analysis showing the peak current of the probe modified electrode (probe concentration: 1 μM) against different target conditions, where NC, C and HSA stand for noncomplementary target, complementary target and human serum albumin, respectively.

increase, without significantly altering the peak potential. Furthermore, the ratio of both the peak currents for a particular scan rate is fairly close to 1 (see Annexure 4 of the ESI†). Using the slope of the plot between the anodic peak current and square root of the scan rate, we have calculated the effective surface area of the working electrode from the Randles–Sevcik equation,[33] which is given as:

$$\text{Slope} = (2.69 \times 10^5) n^{3/2} A D^{1/2} C v^{1/2} \quad (1)$$

where, n is the number of electrons transferred, A is the area of the working electrode, v is the scan rate, D is the diffusion coefficient of the redox probe and C is the concentration of the redox species in the electrolyte. The area, as calculated using the standard diffusion coefficient of $K_3Fe(CN)_6$ (*i.e.* 7.6×10^{-6} $cm^2\ s^{-1}$),[33] is found to be 0.768 cm^2. This, in comparison with the area of the fabricated Ti working electrode (diameter: 2 mm), is significantly higher, and such an increment can be attributed to the Au nanostructures.

Of note, we have evaluated the stability of the bare working electrodes in the working buffer, before performing any biosensing experiments. Towards this, we incubated the electrodes in the test solution (working buffer with the redox couple) for 30 minutes, so as to observe any destabilizing effect of the electrolyte on the Au nanostructures. Cyclic voltammograms of one of the electrodes before and after the incubation step are shown in Annexure 5 of the ESI.† As can be seen, the cyclic voltammograms do not show any significant alteration after the incubation. This is an indication of the electrode's stability in the test solution.

Case study 1: DNA hybridization detection

Towards the targeted DENVCP specific DNA detection, we have used differential pulse voltammetry analysis in the potential range of −0.4 V–+0.4 V. Of note, immobilization of the probe DNA onto the Ti/Au working electrode degrades the electrode's current response (see Annexure 6 of the ESI†). This decrease in the electrode response is a result of the degradation of kinetics at the electrode/electrolyte interface, which is proof of successful immobilization of negatively charged DNA probes. The probe modified electrode was then exposed to different concentrations of the target nucleotide, and the resulting voltammograms are presented in Fig. 6(b). As can be inferred, the peak current decreases with the increase in the target dose, as a result of the decremental reaction kinetics at the working electrode/electrolyte interface. Of note, the target used in this case study has been created using a serial dilution method, as spiked buffer samples. Here, the degradation in kinetics can be explained in terms of the increase in overall negative surface charge density, as a result of target DNA hybridization, which essentially increases the electrostatic barrier seen by the electrons. This degraded kinetics gets translated into a reduced peak current in DPV analysis, which can be correlated to the corresponding surface conditions for establishing a calibration. We have followed a similar approach here to derive a calibration system that would eventually help us in developing a point-of-care system. Fig. 6(c) shows the calibration graph, in the target concentration range of 10 fM–2 μM. Here, the error bars associated with the individual data points correspond to standard deviation values calculated with three identical devices. Of note, beyond 1 μM, even if the target concentration is increased, the electrode's response does not show any appreciable change, indicating saturation against the probe DNA. Such behaviour is expected, given the fact that the working electrode was originally decorated with a 1 μM aliquot of the probe DNA. On the experimental data, we performed a four parameter logistics fit to derive a calibration equation that would analytically describe the electrode's behaviour,[34] and the same is appended in Fig. 6(c). As can be seen, the equation models the system's behaviour with high accuracy, which is indicated by the R^2 value. Using the calibration equation, we further analyzed the reproducibility of the biosensor, wherein we assumed a blind testing protocol. Therein, we exposed the probe modified electrode to a specific target dose and then from the resulting sensor response, we back calculated the target concentration. A comparative analysis between the target dose and the estimated dose is tabulated in Table 2 below. As observed, the estimated dosage closely approximates the original dose, referring to reasonable reproducibility. In addition to this, we have estimated the reproducibility of the sensor by evaluating the response of 5 probe modified electrodes to an identical target dose. The same is presented in Annexure 7 of the ESI.†

Furthermore, we analysed the biosensor's selectivity against interference following the protocol previously explained. As can be seen in Fig. 6(d), the sensor's response to very high concentrations of interfering agents is negligible, whereas to a similar target dose (10 nM), the sensor shows an appreciable change in the peak current. Also, when exposed to the same target dose in the presence of the interfering species, the sensor's response remains almost identical. In addition to this, we have analysed the stability of the biosensor by periodically recording their response over a period of 4 weeks, during which the probe DNA electrodes were stored under refrigeration. The results, as shown in Annexure 5 of the ESI,† show a 16.45% reduction in the device's response (in terms of peak current), indicating reasonable stability. We have been able to detect the target DNA samples using devices that have been stored for 4 weeks. We have further calculated the theoretical limit of detection of the proposed sensor using the 3σ (here, σ is the standard deviation of the blank measurement) method,[35] and it was found to be 0.97 fM. The biosensor accounted for a sensitivity of 20.78 ($\mu A\ \mu M^{-1}$) cm^{-2}.

Table 2 Electrode reproducibility

Target dose	Peak current (μA)	Estimated dose
1 pM	14.12	1.88 pM
100 pM	11.81	117.4 pM
1 nM	9.79	1.67 nM
10 nM	8.49	12.1 nM

Case study 2: working with PCR products

As part of the second case study, in this work, we have used BRCA1 gene specific DNA hybridization, wherein, we have used both wild type and mutant targets. Previously, we have reported about detecting BRCA1 gene specific delAG mutation using an electrochemical immunoassay having doped metal oxide nanofibers.[15] Therein, we had used single stranded probe DNA and single stranded target DNAs with and without the intended mutation. We developed a transduction mechanism based on the differential hybridization between the probe nucleotide and the complementary/ mutated target. Here, we extend our previous findings one step closer to real time applications and perform the experiments with PCR products. In doing so, we evaluate the proposed system's ability in differentiating the complementary targets from the mutated ones.

As part of the experimentation, we decorated the working electrodes with 1 μM of the probe DNA, and the corresponding response was recorded in terms of DPV. The electrodes were then incubated with target DNAs, and allowed to hybridize. The effect of target hybridization on the device's response was estimated using DPV analysis, and the results are shown in Fig. 7. As shown, the normalized change in the peak current can be used as an indicator for differentiating the target DNA into two distinct categories, wild type and mutated (delAG). This can be attributed to the fact that on account of dissimilar binding energies and hybridization coefficients, both the targets give rise to an unequal negative surface charge. This in turn leads to unequal rate kinetics at the working electrode, which manifests in unmatched peak currents. The results are indeed in-sync with our previously reported communication. The outcome was verified using three separate working electrodes, for each target. Furthermore, for each electrode, the device response was recorded three times, for which the corresponding standard deviations are appended as error bars. In the present case, as the probe is complementary to the mutated sequence, the target delAG actually results in a complementary binding, whereas the wild type target DNAs correspond to a two base mismatch. Of note, an identical experimentation can be designed using a probe complementary to the wild type target DNA for demonstration purpose.

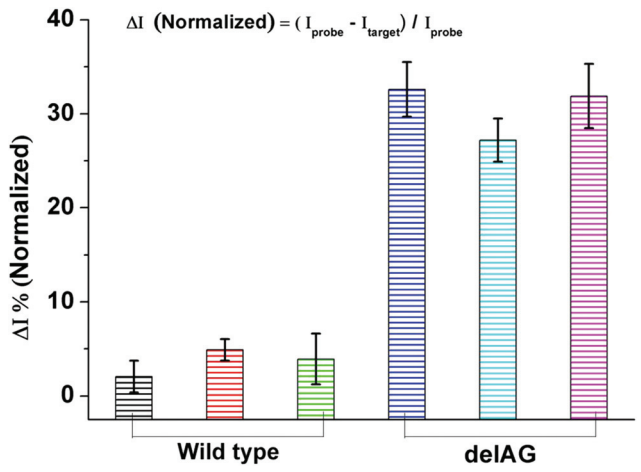

Fig. 7 Bar diagram showing the normalized change in the peak current for PCR modified wild type and mutated target DNAs. Here, delAG (target with mutation) is complementary to the probe DNA.

Case study 3: interfacing with Arduino

As part of the third case study, we have tried to interface the miniaturized platform with an Arduino UNO system, such that a fully automated point of care diagnosis platform can be realized in future. Here, we have used a USB–USB interfacing, and a custom designed data acquisition program, which allows us to collect the sensor data as an excel file (.csv) on a computer. A schematic representation of the same is presented in Annexure 8 of the ESI.† Of note, the Arduino allows us to acquire data as an analog input. As a system limited resolution, a detectable change of 5 mV is required to differentiate any two readings on an Arduino. Accordingly, we have designed a differential amplifier circuit as shown Annexure 8 of the ESI,† with a desired gain factor. This helps us detect the changes in the sensor response (*i.e.* output current), which is in the order of microamperes. Here, upon receiving the analog input from the sensor, Arduino transforms the signal into levels between 0 and 1024, which is then calibrated into the corresponding proportionate voltage values (between 0–5 V). Subsequently, the system response (*i.e.* the current value) is derived using the relationship, $I = V/R$, where I is the sensor response, V is the measured analog voltage and R is the standard load resistor. Furthermore, in the present case, we have used an application namely PLX-DAQ (Parallax Data Acquisition) for data collection. The application enables us to acquire and subsequently access the sensor data (from USB to Excel), using the PLX-DAQ-v2.xlsm worksheet which contains a macro. It is to be noted, that for simplicity, here we have used amperometric measurements (I *vs.* t) for demonstration of the idea, and we intend to extend this to other potentiometric techniques in future.

Conclusions

A miniaturized on-chip electrochemical biosensor for the label-free detection of sub-femtomolar DNA hybridization using nanostructured gold working electrodes is reported. The novelty of this report lies in the efficiency of the fabrication process, the subsequent interfacing mechanism, and the label free sub-femtomolar detection of DNA hybridization. Here the fabrication protocol involved four optical lithographic steps and an electrodeposition step, leading to the formation of Pt pseudo-reference and counter electrodes, and a Ti working electrode with nanoflower like gold. Post gold electrodeposition, the overall electrode surface area is enhanced significantly, as derived using the Randles–Sevcik equation. The probe–DNA immobilization on the working electrode makes use of the gold–thiol self-assembly, which is facile in nature, deprived of any complex chemistry. With respect to DENV

specific consensus primer detection, the sensor results in a wide detection range (10 fM–1 μM), a calculated detection limit of 0.97 fM and a sensitivity of 20.78 (μA μM^{-1}) cm^{-2}. Furthermore, the sensor accounts for reasonable stability against interference and fairly good reproducibility. This generic sensor can be applied for the detection of any DNA hybridization of interest by selecting a different probe–target pair. We have also demonstrated the system's ability for differentiating wild type targets from mutated counterparts with a two base deletion. This is a testament to the system's selectivity. In doing so, we have performed experiments with PCR products, which is a demonstration of the fact that the miniaturized platform can be used for real time applications. In addition to this, the system is equipped with a PDMS layer, that creates a dedicated reaction chamber. The reaction chamber, in addition to ensuring uniformity across devices, reduces the overall sample and reagent volume, needed for the analysis. Furthermore, we have incorporated a micro-USB based electrical interface on the miniaturized platform, which will facilitate easy readout. This will eventually help in developing an on-chip platform for the envisaged point-of-care diagnosis. However, it is to be noted, that the detection of viral RNA requires an RNA extraction step. Also, the use of real time targets involves PCR amplification of the desired locus, as a pre-requisite. Performing such activities on-chip is a challenging task, which we are planning to address categorically such that a fully standalone platform can be realized.

Conflicts of interest

There are no conflicts to declare.

Acknowledgements

The authors acknowledge the Department of Science and Technology (Fund for Improvement of S&T Infrastructure), Government of India and Board of Research in Nuclear Sciences (BRNS), Government of India for funding the research. The authors also acknowledge Dr Rajiv Sarin for providing the del185AG PCR samples.

References

1 S. Bhatt, *et al.*, *Nature*, 2013, **496**, 504–507.
2 S. Cosnier and P. Mailley, *Analyst*, 2008, **133**, 984–991.
3 A. Sassolas, B. D. Leca-Bouvier and L. J. Blum, *Chem. Rev.*, 2008, **108**, 109–139.
4 A. Barhoumi and N. J. Halas, *J. Am. Chem. Soc.*, 2010, **132**, 12792–12793.
5 R. Campos, J. Borme, J. R. Guerreiro, G. Machado, M. F. Cerqueira, D. Y. Petrovykh and P. Alpuim, *ACS Sens.*, 2019, **4**, 286–293.
6 T. G. Drummond, M. G. Hill and J. K. Barton, *Nat. Biotechnol.*, 2003, **21**, 1192–1199.
7 Y. Du, B. J. Lim, B. Li, Y. S. Jiang, J. L. Sessler and A. D. Ellington, *Anal. Chem.*, 2014, **86**, 8010–8016.
8 J. Li and E. C. Lee, *Biosens. Bioelectron.*, 2015, **71**, 414–419.
9 E. Palecek, M. Fojta and F. Jelen, *Bioelectrochemistry*, 2002, **56**, 85–90.
10 H. A. Faria and V. Zucolotto, *Biosens. Bioelectron.*, 2019, **131**, 149–155.
11 M. Manzano, S. Viezzi, S. Mazerat, R. S. Marks and J. Vidic, *Biosens. Bioelectron.*, 2018, **100**, 89–95.
12 D. Fan, Y. Fan, E. Wang and S. Dong, *Chem. Sci.*, 2018, **9**, 6981–6987.
13 M. M. Rahman, Y. J. Kim and J. J. Lee, *J. Electrochem. Soc.*, 2015, **162**(7), B159–B162.
14 S. Tripathy, S. R. K. Vanjari, V. Singh, S. Swaminathan and S. G. Singh, *Biosens. Bioelectron.*, 2017, **90**, 378–387.
15 S. Tripathy, R. Gangwar, P. Supraja, A. N. Rao, S. R. K. Vanjari and S. G. Singh, *Electroanalysis*, 2018, **30**, 2110–2120.
16 S. Tripathy, J. Joseph, S. R. K. Vanjari, A. N. Rao and S. G. Singh, *IEEE Sens. Lett.*, 2018, **2**, 1–4.
17 F. Lucarelli, G. Marrazza, A. P. F. Turner and M. Mascini, *Biosens. Bioelectron.*, 2004, **19**, 515–530.
18 J. Zhang, S. Song, L. Wang, D. Pan and C. Fan, *Nat. Protoc.*, 2007, **2**, 2888–2895.
19 P. A. Rasheed and N. Sandhyarani, *Microchim. Acta*, 2017, **184**, 981–1000.
20 Q. Yi and W. Yu, *J. Electroanal. Chem.*, 2009, **633**, 159–164.
21 N. S. Lopa, *et al.*, *Biosens. Bioelectron.*, 2019, **126**, 381–388.
22 W. Kang, X. Pei, C. A. Rusinek, A. Bange, E. N. Haynes, W. R. Heineman and I. Papautsky, *Anal. Chem.*, 2017, **89**, 3345–3352.
23 E. O. Blair and D. K. Corrigan, *Biosens. Bioelectron.*, 2019, **134**, 57–67.
24 A. Economou, C. Kokkinos and M. Prodromidis, *Lab Chip*, 2018, **18**, 1812–1830.
25 H. I. Peng, C. M. Strohsahl and B. L. Miller, *Lab Chip*, 2012, **12**, 1089–1093.
26 P. Zuo, X. Li, D. C. Dominguez and B. C. Ye, *Lab Chip*, 2013, **13**, 3921–3928.
27 J. Simard, *et al.*, *Nat. Genet.*, 1994, **8**, 392–398.
28 D. Abeliovich, *et al.*, *Am. J. Hum. Genet.*, 1997, **60**, 505–514.
29 S. F. Liu, *et al.*, *Electrochim. Acta*, 2005, **51**, 427–431.
30 W. Cheng, S. Dong and E. Wang, *Chem. Mater.*, 2003, **15**, 2495–2501.
31 S. Chah, J. Yi, C. M. Pettit, D. Roy and J. H. Fendler, *Langmuir*, 2002, **18**, 314–318.
32 D. A. C. Brownson and C. E. Banks, *The Handbook of Graphene Electrochemistry*, Springer-Verlag: London Ltd., 2014, pp. 23–77.
33 A. Purwidyantri, *et al.*, *J. Electrochem. Soc.*, 2017, **164**, B205–B211.
34 M. Khan, A. R. Khan, J. H. Shin and S. Y. Park, *Sci. Rep.*, 2016, **6**, 22676.
35 K. Mahato, P. K. Maurya and P. Chandra, *3 Biotech*, 2018, **8**, 149.